JSR Publications

Available Online

J. Sci. Res. **17** (2), 507-518 (2025)

JOURNAL OF SCIENTIFIC RESEARCH

www.banglajol.info/index.php/JSR

Performance Assessment of Bridgeless Zeta Converter and Solar Energized Zeta Converter Based ACS

S. Mishra[1], S. Singh[2*]

[1]Department of Electrical and Electronics Engineering, Shri Ramswaroop Memorial University, Barabanki-225003

[2]Department of Electrical Engineering, Madan Mohan Malaviya University of Technology, Gorakhpur-273010

Received 21 November 2024, accepted in final revised form 20 February 2025

Abstract

Two important factors to promote energy conservation are to reduce carbon footprint and excessive burden on distribution system. Air conditioning system (ACS) is one such application which is used to provide human comfort and uses excessive energy. In this paper, two configurations namely (one with bridgeless converter and other with solar energy energized converter) are considered for the ACS to reduce losses and promote alternate energy usage. In solar based ACS, Sunlight is tracked and transformed into electrical energy, which is fed to the converter for achieving steady voltage and provided to the inverter that is connected to motor. To determine the feasibility of both the ACSs, these are simulated using MATLAB/Simulink and results are recorded under a range of performance characteristics including torque and speed.

Keywords: Photovoltaic; Zeta converter; Air conditioning system; Power Quality.

doi: https://dx.doi.org/10.3329/jsr.v17i2.77859 J. Sci. Res. **17** (2), 507-518 (2025)

1. Introduction

Requirement for air conditioning systems (ACS) is increasing exponentially to provide human comfort against extreme weather conditions and to protect from rapid change in climatic condition. However, over usage of ACS causes high harmonic pollution (in conventional ACS only) and global warming. Traditionally, ACS is powered by a single phase AC supply and a motor that are impacted by harmonics distortion severely [1-4]. Low power factor and high harmonic content in the input current results in deteriorating power quality which is not good. The standards established by international regulatory agencies such as IEC 61000-3-2 [5,6] are violated in this case. A power converter is placed in between the diode bridge and the motor to reduce the harmonic content in the input current and to maintain almost unity power factor at the front end [7-9]. Various three phase

* *Corresponding author*: Ishikha.singh@gmail.com

inverters are employed to convert dc into ac voltage [10-15]. An off grid and three phase grid tied adaptive logarithmic state feedback control used in digital control system is proposed [10]. A predictive voltage control model with an ideal switching order is reported [11]. Neutral point voltage balancing is accomplished by removing weighing variables through the use of two voltage vector switching modes. For three phase grid tied inverter, a developed virtual phase-current regulation mechanism to decrease the double-line frequency power ripple at dc-link is presented [12]. For multiphase three level neutral point clamped inverters, a hybridized pulse width modulation technique is proposed [13]. Real time diagnostics of single and double open circuit failures of three-phase voltage source inverters is discussed [14]. A method for resolving over voltage issues by independently injecting reactive current into each phase is presented [15].

Zeta converters are flexible and effective dc-dc converter with numerous benefits such as high voltage conversion ratio, continuous input and output current etc. [16-20]. A non-isolated single switch high step-down converter based on a zeta converter has been proposed [16]. The use of an enhanced voltage-mode controller to operate a buck-boost converter based on a zeta converter is demonstrated [18]. A theoretical circuit analysis of the continuous conduction mode, steady-state operation non-isolated dc-dc zeta converter is discussed [19]. Boost zeta dc-dc converter with linked inductors is appropriate to be used in production of new energy [20].

At input side, diode bridge is not required in case of bridgeless configuration. This calls for reduction in total number of conducting devices in a switching cycle as well as overall losses. Bridgeless zeta converters are discussed [21,22]. A bridgeless zeta inverter with its control strategy and dynamic model is presented [21]. The proposed inverter has a bridgeless structure and fewer power components usage makes it compact and reliable. A new electric car charger with integrated supply side power factor pre-regulation based on a bridgeless isolated zeta-Luo converter is proposed in literature [22]. In this, combination of zeta and Luo converter is intended to operate during separate half cycle of supply voltage.

Considering financial, environmental and shortage of fossil fuel aspect, solar power are replacing conventional ac energized ACS. Photovoltaic (PV) array and battery work together to provide electricity to the variable speed drive. With this configuration, a low power UPS connects the utility grid to the variable speed drive as well. Numerous forms of solar-powered air conditioning applications have been covered [23-26]. A distributed algorithm to schedule the heating, ventilation, air conditioning and battery energy storage system in order to address the energy management issue in microgrid is discussed in [23]. In order to leave the impact of energy consumption from the utility grid, PV generation is combined with battery energy storage for air conditioning [24]. A street lighting system that used solar power and a battery as an installed case study in Italy has been discussed [25]. The effects of anthropogenic air pollution on solar resource uptake and PV production are measured [26]. The use of a bidirectional converter has allowed power to flow continuously [27-31].

The literature review highlights the importance of power quality and application of solar energy in ACS in the current era. One cannot limit the use of ACS; thus, the attention

must be directed towards other strategies for raising performance in terms of enhanced power quality in ACS (conventional) or using a different energy source (solar in this case). This paper addresses two such configurations of ACS. Both the ACS has been modeled and examined by using a zeta converter. Further, to highlight the benefits and drawbacks of both ACS, a comparison of these two ACSs has been carried out.

2. System Configuration

Figs. 1 and 2 depict the two ACSs: one with a non-isolated bridgeless zeta converter integrated with the inverter at the front end and the other with solar energized zeta converter. For bridgeless zeta converter (Fig. 1), energy source is a single-phase ac supply. A LC filter is connected to the zeta converter which produces a controlled dc output voltage that is connected to Voltage source inverter (VSI). A Proportional and Integral (PI) voltage controller-1 regulates the front end converter output and keeps it constant regardless of changes in load and input voltage. To obtain the desired output, bridgeless zeta converter output is cascaded to a VSI. Solar powered ACS provides significant voltage gain without the need for a high duty ratio. The MPP controller receives the voltage and current from the PV system to generate pulse width modulation pulses used to drive the zeta converter. Battery is connected to act as the energy source in case of nil solar radiation; thus system is self-sustainable during low intensity. Three phase inverter has been utilized to convert the DC voltage output into AC voltage in both ACS. To operate the ACS, Permanent Magnet Synchronous Motor (PMSM) receives the output of this three phase inverter.

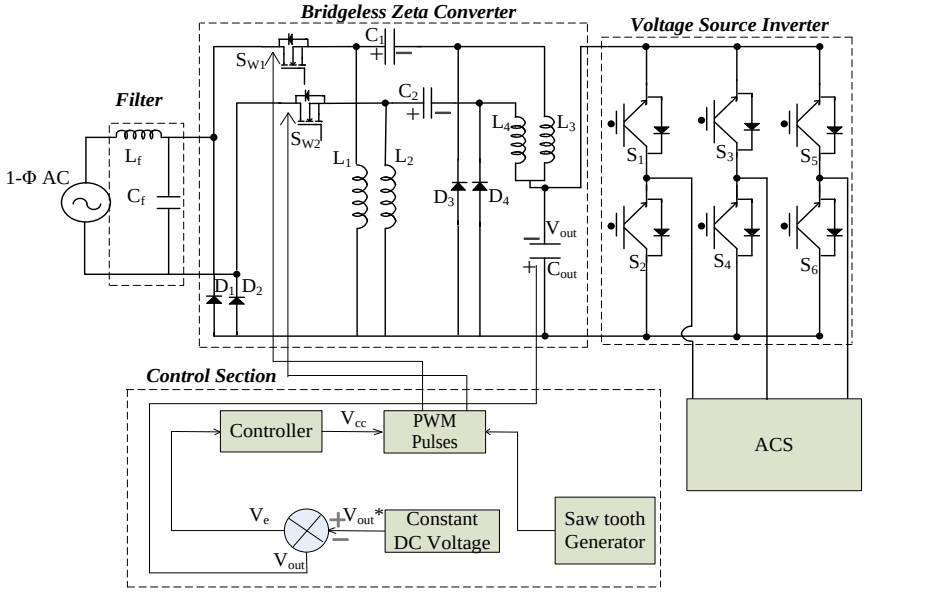

Fig. 1. System configuration of bridgeless zeta converter based ACS.

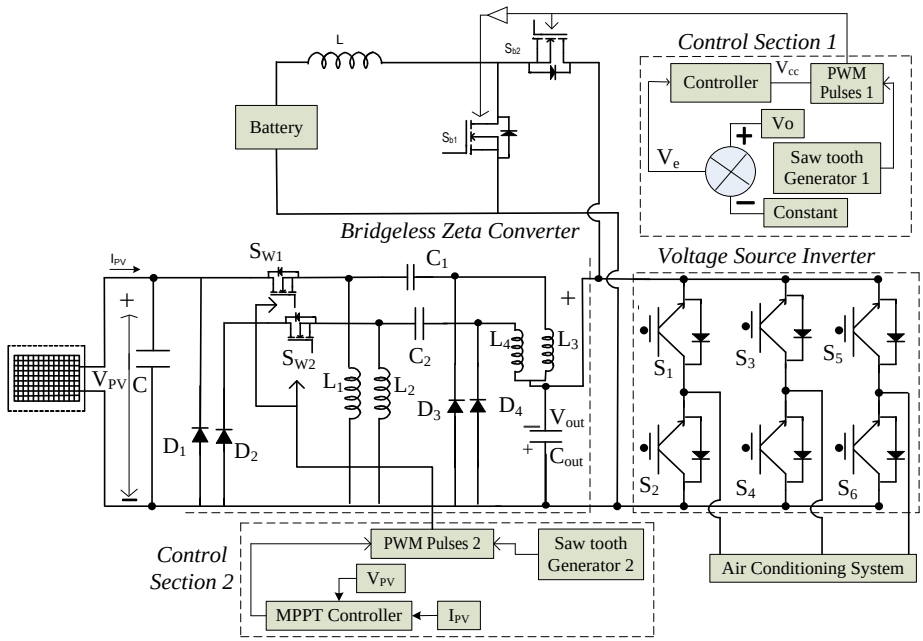

Fig. 2. System configuration of solar energized zeta converter based ACS.

3. Design of ACS

In this section, design of the ACS has been given: (i) Zeta converter based bridgeless ACS and (ii) Solar powered based ACS.

3.1. *Zeta converter based bridgeless ACS*

The ACS is analyzed to present the necessary design equations for modeling, design and component value estimation. Passive components are considered linear, the switches and diodes as optimal and the output filter capacitors as large as necessary to maintain the output voltage constant. As the single phase ac input switching frequency is higher than the fundamental frequency, average quantities during a single switching cycle has taken into consideration.

As the bridgeless zeta converter belongs to the buck-boost converter family, the relationship between the input and output voltages is as:

$$n = \frac{V_{out}}{V_{out}+V_{in}} = \frac{360V}{360V+220V} = 0.62 \quad (1)$$

where V_{in} denotes the input voltage and V_{out} is output DC value.

In order to minimize the ripples in the input ac current, the LC filter on the input side of the bridgeless zeta converter is constructed. The filter's capacitor value (C_{max}) is determined as,

$$C_{\max} = \frac{I_{peak}}{w_c * V_{peak}} \tan(\theta) = \frac{(\sqrt{2} P_{0ut} / V_{in})}{w_c * V_{peak}} \tan(\theta)$$

$$= \frac{(3000W * \sqrt{2})}{314Hz * 220^2 V * \sqrt{2}} \tan(1^\circ) = 6.89\mu F \quad (2)$$

In this case, θ is the angle between V_{peak} and I_{peak}, which stands for the maximum value of single phase ac voltage and current, respectively. As a result, the filter capacitor's value is 6.7μF.

Permitting for the supply system's impedance gives the inductor value, which is determined by,

$$L_{eq} = \frac{1}{4\pi^2 f_c^2 c_f} = \frac{1}{4*(3.14)^2*2000^2 Hz*6.7\mu F} = 946mH \quad (3)$$

Where, f_c is the interrupt frequency.

The input side inductor value is taken into account for the permitted ripple current of i_{in},

$$L_1 = L_2 = \frac{v_{in} n}{\eta i_{in} f_s} = \frac{220V*0.62}{0.3*13.63A*20000Hz} = 1.67mH \quad (4)$$

The input current value is computed as,

$$i_{in} = \frac{P_{out}}{V_{in}} = \frac{3000W}{220V} = 13.63A \quad (5)$$

The inductor at the output side is calculated as,

$$L_3 = L_4 = \frac{V_{out}(1-n)}{\Delta I_{L2} f_s} = \frac{360V*(1-0.62)}{1.67A*20000Hz} = 4.1mH \quad (6)$$

Here ΔI_{L2} is taken as 20 % of $I_{out.}$

$$i_{out} = \frac{P_{out}}{V_{out}} = \frac{3000W}{360V} = 8.33A \quad (7)$$

For an admissible ripple voltage of κ=10 % of the output dc voltage, the middle capacitance is designed as,

$$C_1 = C_2 = \frac{I_{out} n}{k V_{out} f_s} = \frac{8.33A*0.62}{0.1*360V*20000Hz} = 717\mu F \quad (8)$$

Second order harmonics is reduced with the use of an output capacitor. The design is as,

$$C_{out} = \frac{I_{out}}{2w\Delta V_{out}} = \frac{8.33A}{2*314Hz*7.2V} = 1.84mF \quad (9)$$

3.2. *Solar powered zeta converter ACS*

Zeta converter receives solar energy from the solar PV array. Table 1 provides the design parameters of solar array. Zeta converters are primarily designed to operate in two modes: first, when the switch S_w is turned on and second, when switch is turned off. The design of zeta converter is same as bridgeless zeta converter as discussed in previous section. Therefore, the value of input inductor, output inductor, middle capacitor and output capacitor comes out to be same as before.

Table 1. PV parameters for the proposed solar powered ACS.

Parameter	Designed values
Short circuit current	8.21A
MPP current	7.61A
Open circuit voltage	32.9V
MPP voltage	26.3V
Number of cells in a module	54
Number of series connected modules	12

4. Assessment of ACS Performance

Various conditions have been simulated in order to assess the performance of both ACSs. In case (i), different power quality indicators are calculated and analyzed to indicate enhanced power quality even in the condition of input voltage variation. The DC voltage is maintained at almost 360 V when the input voltage varies from 200 V to 240 V. In scenario (ii), the zeta converter is utilized to acquire the performance of a solar energized ACS for different irradiation levels. Comparative studies of the different simulation findings of solar-energized ACS using a zeta converter and ACS using a bridgeless zeta converter have been conducted.

4.1. *Assessment of bridgeless zeta converter ACS*

4.1.1. *At input voltage of 220 V*

At 220 V input voltage, performance metrics are recorded and displayed in Fig. 3a. The maximum input current is 16.13 A, while the reported dc output voltage is 360 V. The electromagnetic torque is found to vary between 2.7 Nm and 3.5 Nm, while the rotor speed is reported to be 1955 rpm, as shown in Fig. 3a. The current wave shape and harmonic spectra at 220V are shown in Fig. 3b.

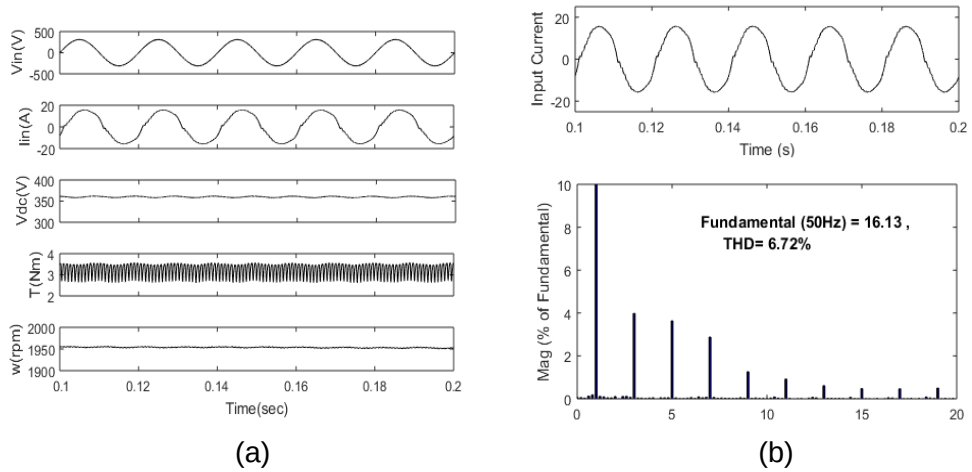

Fig. 3. Performance and harmonic spectra of the ACS at 220 V input voltage.

4.1.2. *At input voltage of 200 V*

To assess the control of the ACS, a voltage of 200 V is applied and the same performance metrics are noted under these voltage conditions. The maximum input current detected is 20.66 A, which is marginally higher than the 220 V operation. The electromagnetic torque ranges from 2.7 Nm to 3.5 Nm, clear from Fig. 4a. The current waveform at and its harmonic spectra at 200 V are displayed in Fig. 4b.

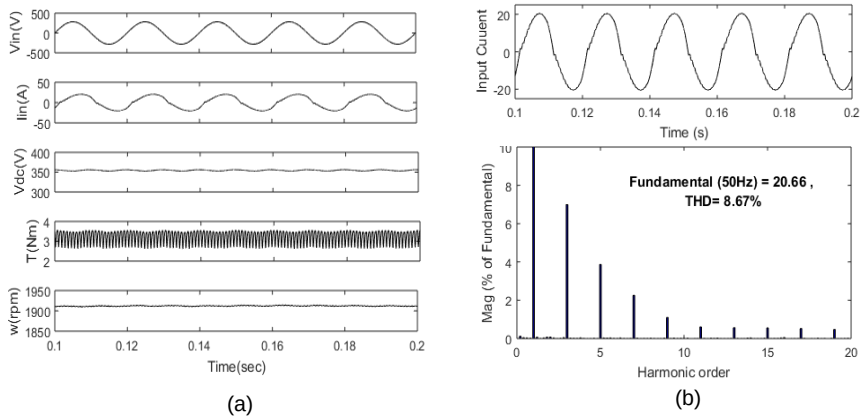

Fig. 4. Performance and harmonic spectra of the ACS at 200V input voltage.

4.1.3. *At input voltage of 240 V*

The input current is 13.56 A (max) at an input voltage of 240 V, as illustrated in Fig. 5a, while the dc output voltage remains constant up to 360 V. 1984 rpm is the obtained rotor

speed and the electromagnetic torque ranges again from 2.7 to 3.5 Nm. The current waveform in this overvoltage situation is displayed in Fig. 5b.

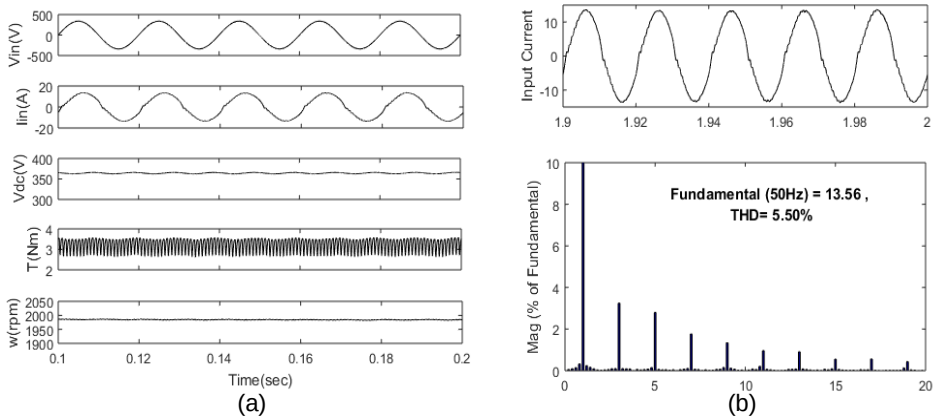

Fig. 5. Performance and harmonic spectra of the ACS at 240 V input voltage.

The different performance metrics of the bridgeless zeta converter with ACS under different input supply voltage variations are displayed in Table 2.

Table 2. Performances parameters of ACS using zeta converter.

Input Voltage(rms) V_{in} (V)	Input Current (max) I_{in} (A)	Output Voltage V_{dc} (V)	Torque (Nm)	Speed (rpm)	THD (%)	PF
200	20.66	360	2.7-3.5	1912	8.67	0.986
210	18.78	360	2.7-3.5	1924	7.23	0.987
220	16.13	360	2.7-3.5	1955	6.72	0.988
230	14.17	360	2.7-3.5	1963	6.08	0.995
240	13.56	360	2.7-3.5	1984	5.5	0.998

The rotor speed remains nearly constant under different input voltages with harmonic distortion falling within acceptable bounds.

4.2. *Assessment of solar-powered ACS*

The solar energy is clean, readily available, affordable, and produces fewer carbon emissions. Thus, as illustrated in Fig. 2, an ACS with a zeta converter, battery backup and solar energy as input has been built. In order to simulate the ACS under various solar irradiation conditions, performance metrics have been measured including torque, speed, battery voltage, battery current and PV voltage.

4.2.1. *At 1000 W/m² solar irradiation*

The data is recorded as indicated in Fig. 6 for PV voltage, PV current, battery voltage, battery current, zeta converter voltage, rotor speed and electromagnetic torque. The battery voltage is 326 V, the battery current clearly swings from -2.6 A to -1.6 A and the zeta converter voltage is kept at 360 V. The PV voltage is observed to be 243 V while the PV current is 8.4 A. Additionally, it is found that the rotor speed is 1874 rpm and the electromagnetic torque ranges from 2.3 to 3.6 Nm.

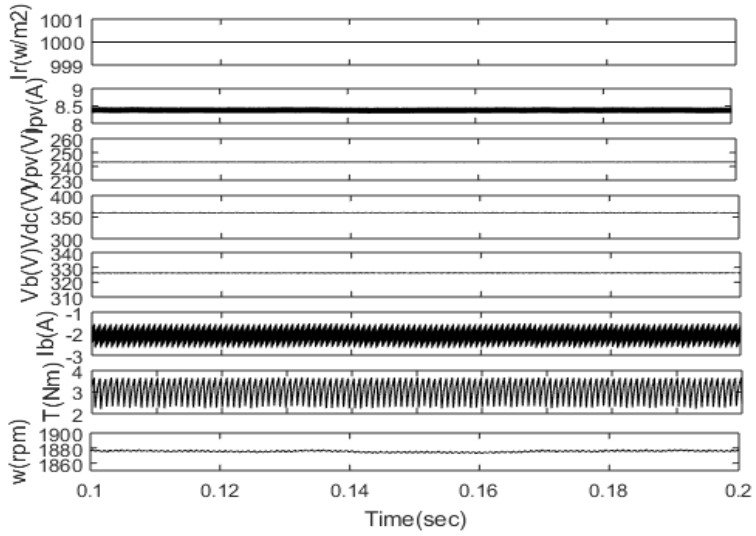

Fig. 6. PV voltage- PV current, dc output voltage, battery voltage, torque and speed at 1000 W/m^2 of Sun intensity

4.2.2. *At 500 W/m² solar irradiation*

The input side solar irradiation is now reduced to 50 % and the performance data such as battery voltage, battery current, rotor speed, electromagnetic torque, zeta converter voltage and PV voltage and current are obtained as illustrated in Fig. 7. Battery voltage is 323.8 V and the battery current swings from 1.6 A to 2.4 A, the PV voltage is slightly dropped to 240 V and the zeta conversion voltage is 360 V. Additionally, the rotor speed is 1874 rpm and the electromagnetic torque also fluctuates between 2.3 and 3.6 nm. With the decreasing amount of solar radiation, ACS is now powered by battery.

4.2.3. *At nil solar irradiation*

Further solar radiation is kept to 0 and the performance parameters such as battery voltage, current, rotor speed, electromagnetic torque and PV voltage and current are illustrated in Fig. 8. It is visible from the result that the battery voltage remains constant and the current

swings from 1.95 A to 3.1 A. The PV voltage and current are 0 in this case. Also, the electromagnetic torque varies from 2.3 Nm to 3.6 Nm and the rotor speed is 1880 rpm.

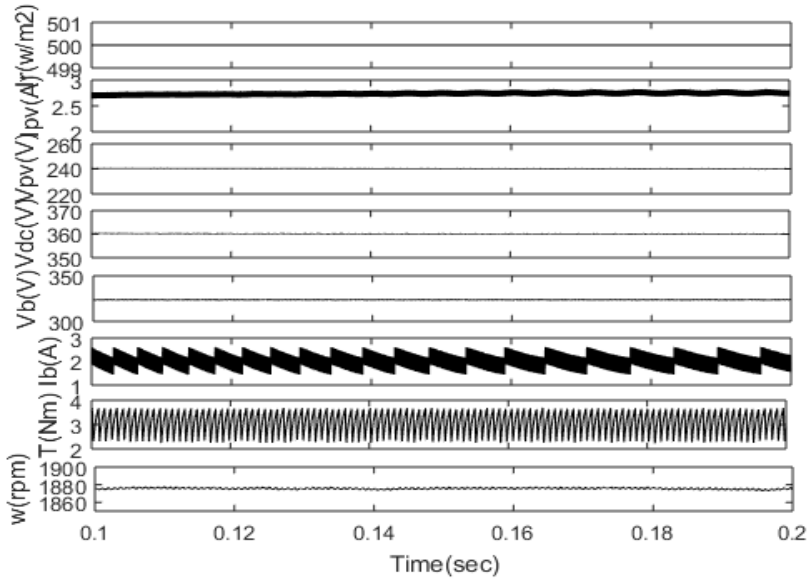

Fig. 7. PV voltage- PV current, dc output voltage, battery voltage, torque and speed at 500 W/m^2 of Sun intensity.

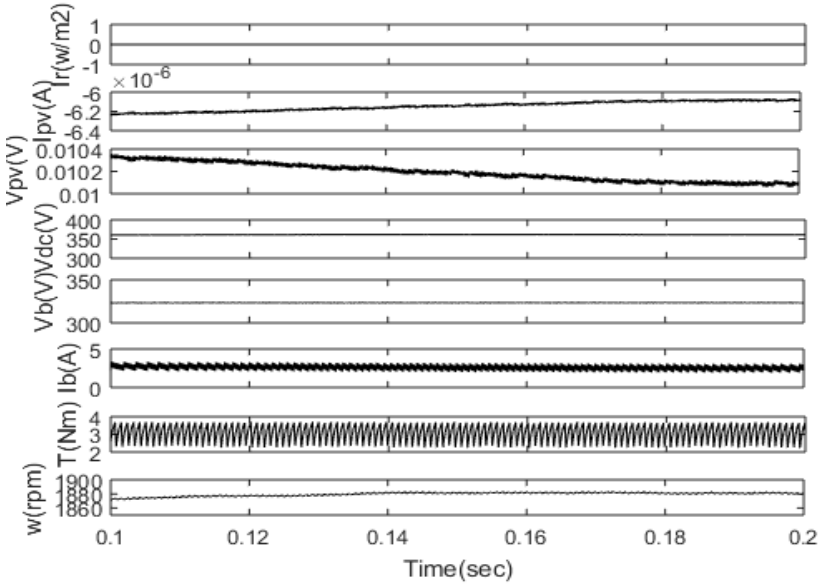

Fig. 8. PV voltage- PV current, dc output voltage, battery voltage, torque and speed at 0 W/m^2 of Sun intensity.

The performance characteristics of the ACS with zeta converter under varied solar irradiation ranging from 1000 W/m^2 to zero (in the absence of the Sun) are summarized in Table 3. In case of scarcity of solar energy, battery powers the system, maintaining a steady voltage and driving the motor at the necessary speed. The PV current decreases due to low intensity as the solar irradiation drops to 500 W/m^2, the voltage of the zeta converter is constant at 360 V. The system is self-sufficient and has excellent control even under conditions of low or no solar radiation.

Table 3. Performances parameters of ACS using zeta converter.

S.No	Intensity (W/m^2)	PV voltage (V)	PV current (A)	Zeta converter voltage (V)	Battery voltage (V)	Battery current (A)	Speed (rpm)	Torque (N-m)
1	1000	243	8.4	360	326	-2.6 to -1.6	1874	2.3-3.6
2	800	243	6.32	360	324	-1.6 to 1.6	1876	2.3-3.6
3	500	240	2.8	360	323.8	1.6 to 2.4	1874	2.3-3.6
4	200	240	2.1	360	323.6	0 to 1.5	1878	2.3-3.6
5	0	0	0	360	323.5	1.95 to 3.1	1880	2.3-3.6

5. Conclusion

The performance of solar energized and bridgeless zeta converters is investigated under a range of operational conditions to show reliability and ruggedness. Both the converters used in the two configurations have been operated in DCM. Bridgeless zeta converter-based ACS has performed satisfactorily with low harmonic distortion of input current and unity power factor. The adaptability and usefulness of both the ACSs has been verified and tested at various operating conditions. On the other hand, solar powered ACS provides low carbon emissions, self-sufficiency and minimal electromagnetic torque variation. For the sake of a better future and environment, solar energized ACS has the potential to replace the current ACS.

References

1. X. Chen, K. Li, Z. Mi, and F. Wang, IEEE Trans. Industry Applicat. **60**, 3 (2024). https://doi.org/10.1109/TIA.2024.3365455
2. B. K. Oleiwi and A. H. Sabry, IEEE Embedded Syst. Lett. **16**, 2 (2024). https://doi.org/10.1109/LES.2023.3348705
3. T. Yano and D. M. Sako, IEEE Access **12** (2024). https://doi.org/10.1109/ACCESS.2024.3367954
4. S. Mishra and S. Singh, J. Sci. Res. **14**, 1 (2022). https://doi.org/10.3329/jsr.v14i1.54429
5. Limits for Harmonic Current Emissions, International Electrotechnical Commission Standard, IEC-61000-3-2 (International electrotechnical Commission, 2004).
6. 519-2014 - IEEE Recommended Practice and Requirements for Harmonic Control in Electric Power Systems (IEEE, 2014). https://doi.org/10.1109/IEEESTD.2014.6826459
7. Z. Qi, M. B. Hossain, M. R. Islam, M. A. Rahman, and R. Raad, IEEE Access **12**, 101228 (2024). https://doi.org/10.1109/ACCESS.2024.3424872

8. M. K. Badapanda, A. Tripathi, R. Upadhyay and M. Lad, IEEE Trans. Power Electron. **38**, 6 (2023). https://doi.org/10.1109/TPEL.2022.3233257
9. N. Yadav, N. Hassanpour, A. Chub, A. Blinov, and D. Vinnikov, IEEE J. Emerging Selected Topics Power Electron. **12**, 2 (2024). https://doi.org/10.1109/JESTPE.2024.3354843
10. W. X. Xiao, G. R. Jiang, J. K. Mao, F. Xie, B. Zhang, D. Y. Qiu, and Y. F. Chen, IEEE Trans. Circuits Systems—II: Express Briefs **71**, 6 (2024). https://doi.org/10.1109/TCSII.2024.3353491
11. Y. Wang, Y. Yang, S. Chen, R. Chen, J. Hu, W. Wu, Y. Wang, H. Yang, L. Zhou, and J. Rodriguez, IEEE Trans. Power Electron. **39**, 2 (2024). https://doi.org/10.1109/TPEL.2023.3333357
12. A. Liu, C. Hou, M. Zhu, Y. Wen, and Y. Cai, IEEE Trans. Industrial Electron. **71**, 10 (2024). https://doi.org/10.1109/TIE.2024.3360617
13. A. Lewicki, D. Kondratenko, and C. I. Odeh, IEEE Trans. Industrial Electron. **71**, 8 (2024). https://doi.org/10.1109/TIE.2023.3321999
14. Y. Luo, Li. Zhang, C. Chen, K. Li, and K. Li, IEEE Trans. Power Electron. **39**, 6 (2024). https://doi.org/10.1109/TPEL.2024.3371452
15. J. I. Iñiguez, J. N. Duarte, A. Camacho, J. Mire, and M. Castilla, IEEE Trans. Industrial Electron. **71**, 10 (2024). https://doi.org/10.1109/TIE.2024.3349525
16. H. Ghojavand and E. Adib, IEEE Trans. Industrial Electron. **38**, 4 (2023). https://doi.org/10.1109/TPEL.2022.3232388
17. X. Sun, D. Rong, and N. Wang, IEEE Trans. Industrial Electron. **71**, 7 (2024). https://doi.org/10.1109/TIE.2023.3299032
18. C. Y. Chan, IEEE Trans. Circuits Systems—II: Express Briefs **71**, 3 (2024). https://doi.org/10.1109/TCSII.2024.3462215
19. M. K. Kazimierczuk, F. Corti, G. M. Lozito, and A. Reatti, IEEE Access **12**, 2635 (2024). https://doi.org/10.1109/ACCESS.2023.3347750
20. X. Fang, X. Lai, X. Wang, and H. Zhao, CPSS Trans. Power Electron. Applicat. **9**, 2 (2024). https://doi.org/10.24295/CPSSTPEA.2024.00001
21. B. Han, S.W. Jo, N.G. Kim, J. S. Lai, and M. Kim, IEEE Trans. Power Electron. **36**, 6 (2024).
22. R. Kushwaha and B. Singh, IEEE Trans. Industry Applicat. **57**, 1 (2021). https://doi.org/10.1109/TIA.2020.3036019
23. J. Ma and X. Ma, IEEE Trans. Industrial Informatics **19**, 12 (2023). https://doi.org/10.1109/TII.2023.3248122
24. D. Das, B. Singh, and S. Mishra, IEEE Trans. Consum. Electron. **69**, 2 (2023). 10.1109/TCE.2022.3215557
25. E. Belloni, A. Massaccesi, C. Moscatiello, and L. Martirano, IEEE Trans. Industr. Applicat. **60**, 3 (2024). https://doi.org/10.1109/TIA.2024.3351091
26. H. Liu, Y. Sun, C. Tan, C. Ho, L. Zhao, and A. Hove, IEEE J. Photovoltaics **13**, 6 (2023). https://doi.org/10.1109/JPHOTOV.2023.3317636
27. P. Muthukumar, M. V. Kumar, and C. S. Chin, IEEE Access **12**, 28710 (2024). https://doi.org/10.1109/ACCESS.2024.3360267
28. H. Gaied, A. Flah, H. Kraiem, and L. Prokop, IEEE Access **12**, 94323 (2024). https://doi.org/10.1109/ACCESS.2024.3403769
29. J. Huang, H. Han, G. Xu, X. Liu, W. Xiong, and M. Su, IEEE Trans. Industrial Electron. **71**, 2 (2024). https://doi.org/10.1109/TIE.2023.3262870
30. X. Han, Y. Liao, and D. Yang, IEEE Trans. Circuits Systems—II: Express Briefs **71**, 6 (2024). https://doi.org/10.1109/TCSII.2024.3360703
31. C. P. Ragasudha and S. Hemamalini, IEEE Access **12**, 14499 (2024). https://doi.org/10.1109/ACCESS.2024.3357726